Available online at www.sciencedirect.com
ScienceDirect
Journal of the European Ceramic Society 27 (2007) 4685–4695
www.elsevier.com/locate/jeurceramsoc

On the surface morphology of solution annealed $Co_{1-x}O$–MgO—Effects of directional dislocation exposure and $Co_{1-x}O$ condensation

Chang-Ning Huang [a], Pouyan Shen [a,*], Kuang-Yeu Hsieh [b]

[a] *Institute of Materials Science and Engineering, National Sun Yat-sen University, Kaohsiung, Taiwan, ROC*
[b] *Emerging Central Laboratory, Macronix International Co., Hsinchu, Taiwan, ROC*

Received 9 November 2006; received in revised form 1 March 2007; accepted 11 March 2007
Available online 6 June 2007

Abstract

The sintered $Co_{1-x}O$ ceramics with or without 20 mol% MgO solid solution in the rock salt type structure were annealed in the temperature range of 400–1500 °C in air for surface morphology development study. Electron microscopic observations indicated the MgO component considerably suppressed the thermal etching and the nucleation of the Co-rich spinel as expected. Surprisingly, prolonged annealing at 1500 °C caused anisotropic development of the {1 1 1}/{1 0 0}-faceted etch pits/hillocks from the cubic crystal system, which can be rationalized by the predominant exposure of ⟨1 1 0⟩ oriented dislocations on the {1 1 1} surfaces. Meanwhile, sublimation–condensation at this temperature caused cube-like $Co_{1-x}O$ crystallites to deposit preferentially on the (1 0 0) surface following parallel or 45° off crystallographic relationship via Brownian motion of the crystallites.

Keyword: Thermal etch pits

1. Introduction

The motivation of this research was to demonstrate, by high temperature annealing experiments, that the solid solution of a cubic crystal system could have rather anisotropic surface morphology due to the combined effects of directional dislocation exposure and a sublimation–condensation process of the relatively volatile component upon thermal etching.

Anisotropic crystals are expected to exhibit directional dissolution in acidic solutions or upon thermal exposure. For example, chemical etching of the hexagonal willemite (α-Zn_2SiO_4) single crystals in acidic aqueous solution showed the dissolution rates along specified directions have the following relationship: $[0\,0\,0\,1] > \langle 1\,0\,\bar{1}\,0\rangle \geq \langle 1\,1\,\bar{2}\,0\rangle$ for pH < 2, but the order was reversed for pH > 2.[1] The dissolution inhibitors, either inherent from natural minerals or added on purpose in solution, tend to accumulate at dislocation outcrops and maintain the near-surface undersaturation of willemite, thus allowing etch pits to develop at these high energy sites on (0 0 0 1) surface.[2] These inhibitors can also cause etch hillocks in areas away from dislocation outcrops on (0 0 0 1) surface[3]. Chemical etching of another hexagonal single crystal, i.e. apatite,[4] in acidic aqueous solution also showed the opening of dislocation etch pits on basal planes. The dissolution rates along the principal directions of the apatite have the following relationship $[0\,0\,0\,1] > [1\,1\,\bar{2}\,0] > [1\,0\,\bar{1}\,0]$ for pH 0–1, but the order was reversed for pH > 3.[4] In general, anisotropic dissolution of these hexagonal crystals can be attributed to the active lattice sites and dislocation exposure to specific surfaces.[1]

On the other hand, thermal exposure of the willemite (0 0 0 1) surface at 1250 °C typically caused shallow hexagonal pits nucleation at dislocation outcrops beneath a surface-premelt Si-rich layer, and the formation of hillocks at etch pit centers,[5] in accordance with the inhibition effect of impurities at dislocation outcrops. By contrast, thermal etching of the polycrystalline willemite in the temperature range of 1050–1350 °C caused rapid grooving at grain boundaries besides anisotropic etching in crystals.[6] The grooves and ridges near the grain boundaries became obscured subsequently due to deposition under the influence of capillarity effect. Thermal etching of the exposed grains also caused faceted pores and surface ledges, which were more or less dragged with dislocation outcrops.[6] Furthermore, Mn^{2+} dopant was found to be an effective inhibitor for the thermal etching at dislocation outcrops and sub-grain boundaries.[6] This

* Corresponding author. Tel.: +886 7 5252000 4060; fax: +886 7 5254099.
E-mail address: pshen@mail.nsysu.edu.tw (P. Shen).

0955-2219/$ – see front matter © 2007 Elsevier Ltd. All rights reserved.
doi:10.1016/j.jeurceramsoc.2007.03.035

point is of concern to thermal stability of zinc orthosilicates in glaze or glass ceramics and degradation of phosphorescence materials, e.g. Mn-doped and (Mn, As)-codoped α-Zn_2SiO_4 in modern CRT displays[7] upon electron-beam heating.

Here we report the surface morphology development of solution annealed $Co_{1-x}O$–MgO ceramics focusing on the underlying effects of directional dislocation exposure on specific surface, and the condensation–deposition of cube-like $Co_{1-x}O$ crystallites on specific surface/ledge. Hopefully, the thermal stability of rock salt type catalytic materials[8] at high temperatures can be better understood.

2. Experimental procedure

$Co_{1-x}O$ (Cerac 99.9%, 2 μm) and MgO (Cerac 99.9%, 5 μm) powders in 8:2 molar ratio (denoted as C8M2) were ball milled in alcohol, oven dried at 100 °C, and then dry pressed at 650 MPa to form pellets ca. 5 mm in diameter and 2 mm in thickness. The C8M2 and undoped $Co_{1-x}O$ pellets were dry pressed under the same condition, and then sintered at 1600 °C for 5 h in air followed by quenching in air to form compositionally homogeneous solid solution. These specimens were further annealed at 1500 °C for 10 min up to 12 h in air, in order to

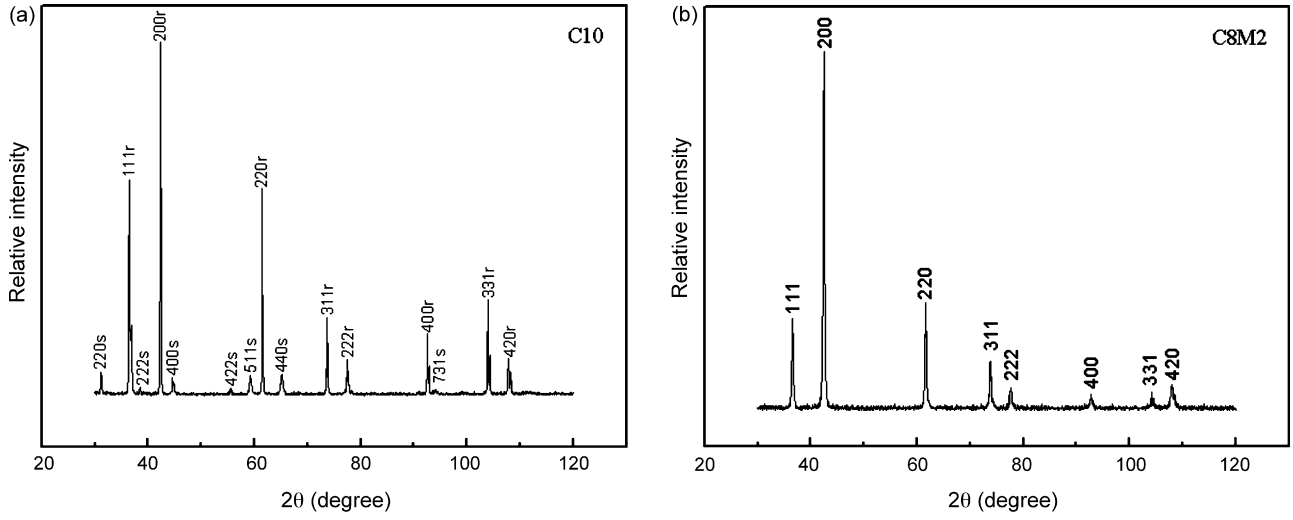

Fig. 1. XRD trace (Cu Kα) of (a) $Co_{1-x}O$ sample with considerable amount of spinel phase (denoted as s) besides the predominant rock salt type phase (denoted as r) and (b) C8M2 sample of rock salt type solid solution with rather limited amount of spinel phase according to AEM. Both samples were sintered at 1600 °C for 5 h and then cooled in air.

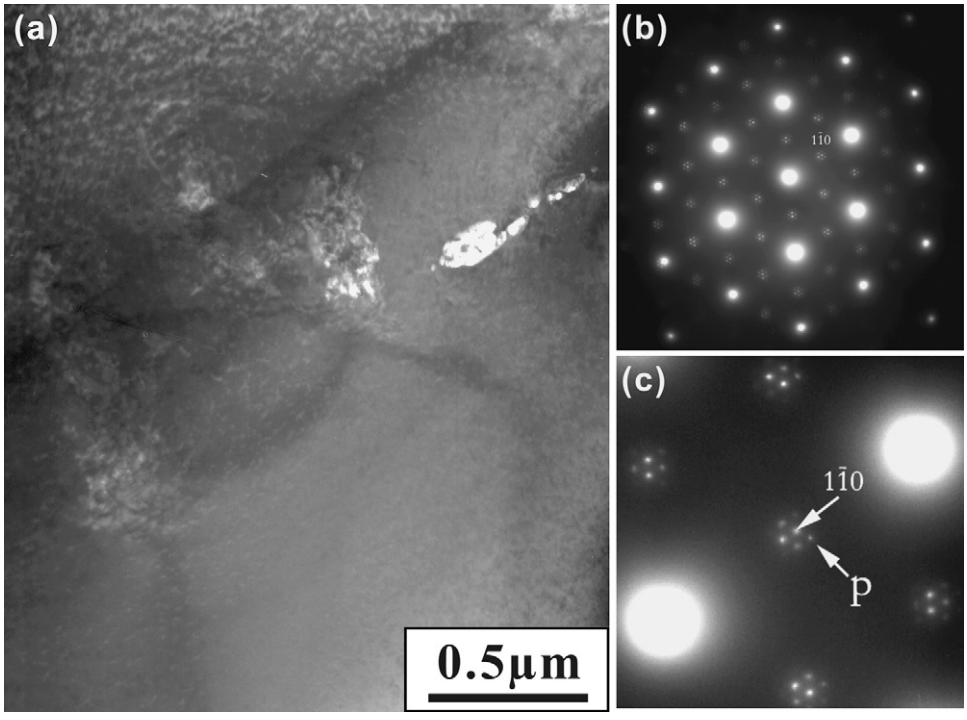

Fig. 2. TEM of the paracrystalline spinel phase in the sintered C8M2 sample subject to thermal etching at 1500 °C for 10 min: (a) DFI ($g = 1\,\bar{1}\,0$ of spinel denoted as s), (b) SAED pattern in [1 1 1] zone axis and (c) magnified from (b) to show paracrystal diffraction (denoted as p) around $1\,\bar{1}\,0$s.

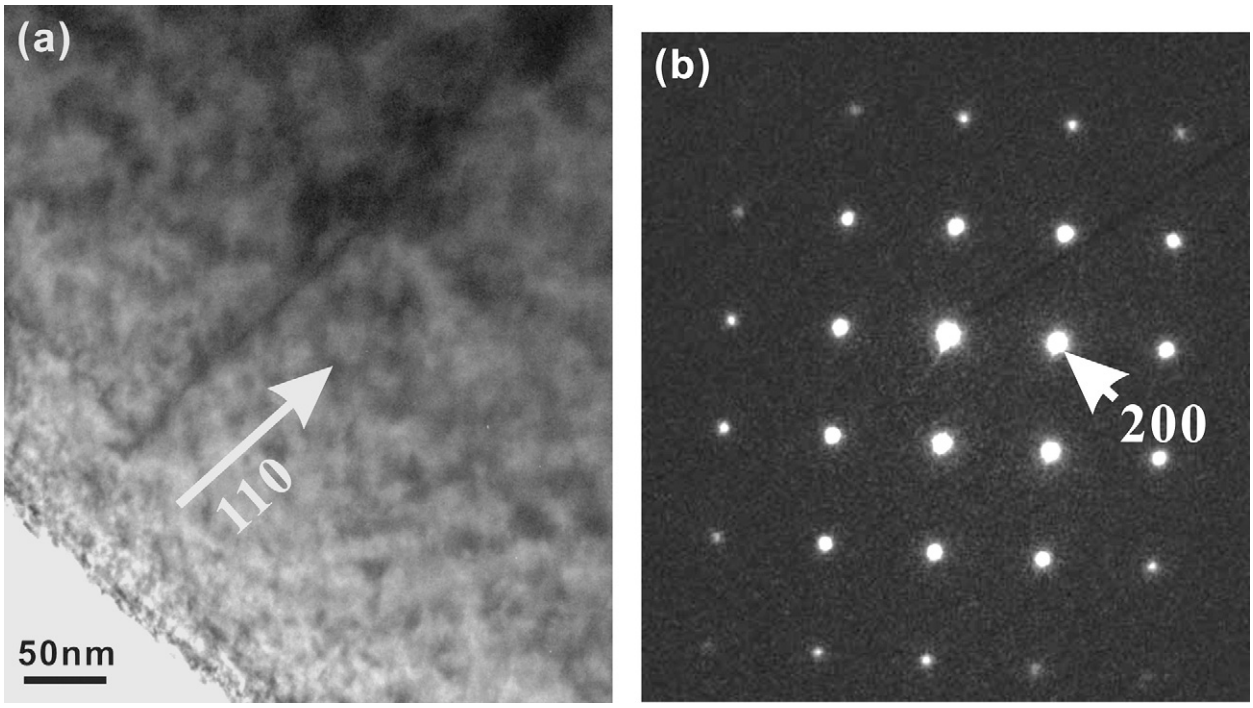

Fig. 3. TEM (a) BFI and (b) SAED pattern in [0 0 1] zone axis of the sintered C8M2 sample subject to thermal etching at 1500 °C for 10 min showing dislocations with line vector parallel to ⟨1 1 0⟩, as the case in C1M9 sample reported in ref.[10]

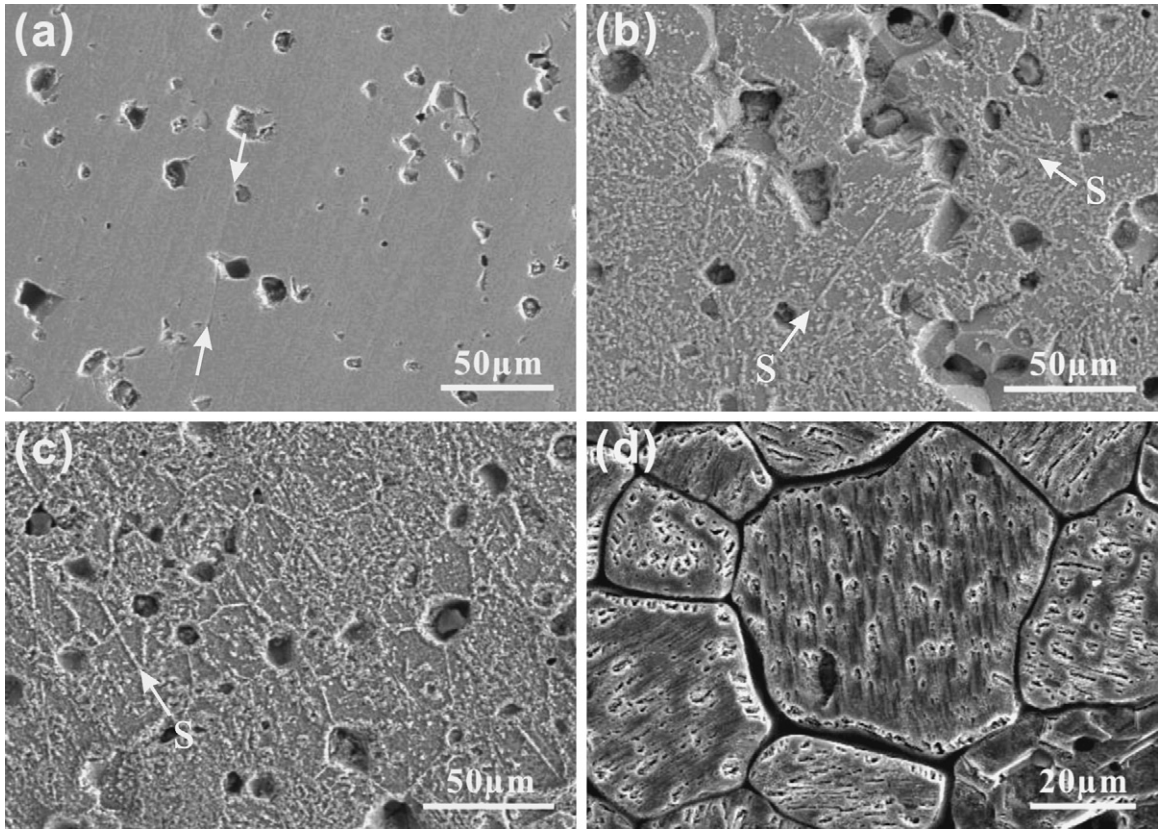

Fig. 4. SEM (SEI) of the sintered $Co_{1-x}O$ sample subject to thermal etching at (a) 400 °C, (b) 800 °C, (c) 1100 °C and (d) 1500 °C for 10 min, showing considerable etching along grinding scratch (denoted by an arrow) in (a); formation of Co-rich (bright) spinel phase (denoted as s) along step ledges in (b) and (c) (cf. text); and extensive development of etch pits and grain boundary grooving in (d).

study the development of the surface morphology and defect clusters.

X-ray diffraction (XRD, Cu Kα, 40 kV, 30 mA, at 0.05° and 3 s per step from 2θ angle of 30° up to 120°) was used to identify the phases of the fired specimens. Thin sections of the sample thermally etched at 1500 °C for 10 min was Ar-ion milled to electron transparency for transmission electron microscopy (TEM, JEOL 3010 instrument at 300 kV) characterization of defect microstructure based on bright field image (BFI) and selected area electron diffraction (SAED) pattern. Scanning electron microscopy (SEM, JSM-6400, 20 kV) coupled with point-count energy dispersive X-ray (EDX) analysis was used to observe the surface morphology of the thermally etched ceramics.

3. Results

3.1. Phase and defect identification

XRD indicated that the $Co_{1-x}O$ ceramic sample sintered at 1600 °C for 5 h contain the spinel phase besides the predominant protoxide of rock salt type structure (Fig. 1a). The spinel phase was formed during cooling in view of the oxidation of $Co_{1-x}O$ to form $Co_{3-\delta}O_4$ spinel below ca. 900 °C.[9] By contrast, the C8M2 ceramic sample fired under the same condition showed only rock salt type solid solution in the XRD trace (Fig. 1b). Apparently, the solid solution of MgO in $Co_{1-x}O$ has suppressed its oxidation upon cooling in air to form the spinel phase.

TEM revealed minor paracrystalline spinel phase in the C8M2 ceramic sample subjected to thermal etching at 1500 °C for 10 min (Fig. 2). The BFI and SAED pattern of the protoxide in this specimen (Fig. 3) further revealed dislocations, which have line vector parallel to ⟨1 1 0⟩ of the rock salt structure. The same dislocation line vector was observed in our previous study of the fired C1M9 polycrystals.[10]

3.2. Surface morphology of thermally etched $Co_{1-x}O$ versus C8M2 ceramics

SEM indicated that the sintered $Co_{1-x}O$ ceramic sample suffered considerable thermal etching along the grinding scratches when annealed at 400 °C for 10 min (Fig. 4a). Upon annealing at 800 or 1100 °C for 10 min (Fig. 4b and c), the Co-rich spinel was developed along the terrace ledges. Thermal etch pits and grain boundary grooves were clearly developed when the sintered $Co_{1-x}O$ sample was annealed at 1500 °C for 10 min (Fig. 4d).

By contrast, the sintered C8M2 ceramic sample subject to annealing at 400 °C for 10 min showed negligible thermal etch-

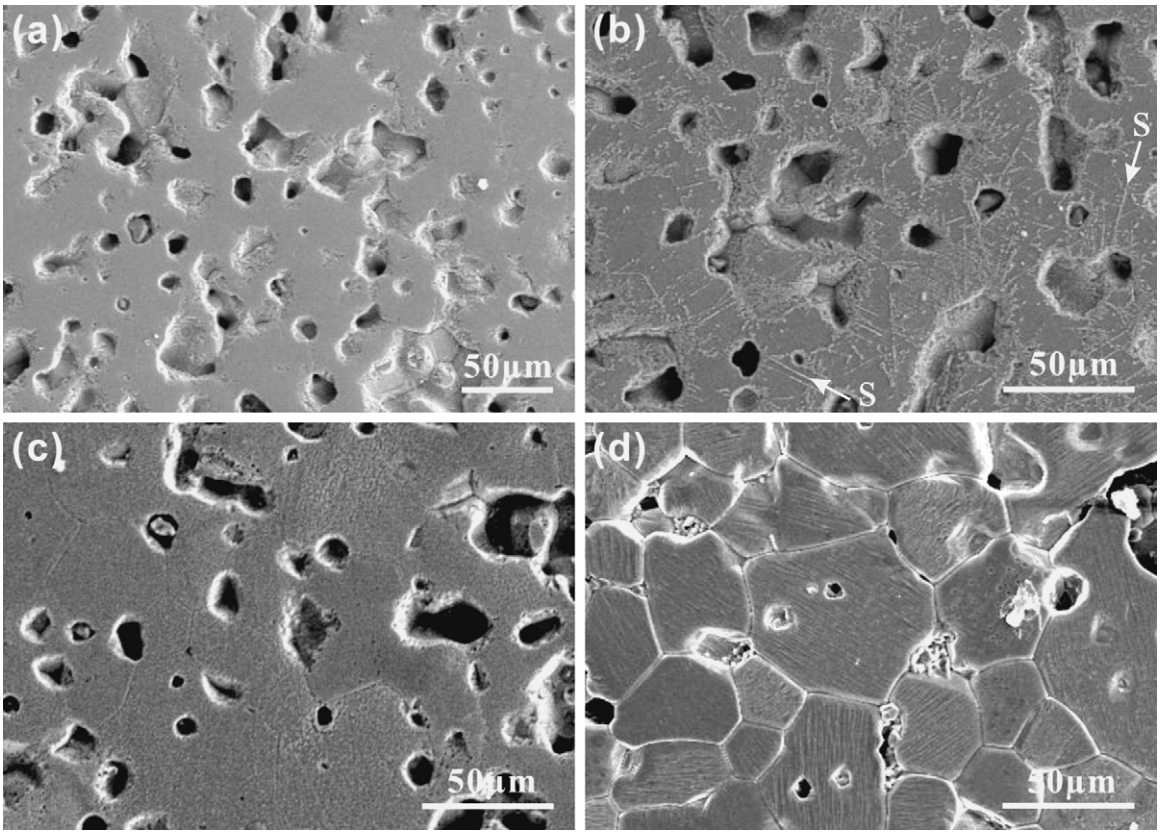

Fig. 5. SEM (SEI) of the sintered C8M2 sample subject to thermal etching at (a) 400 °C, (b) 800 °C, (c) 1100 °C and (d) 1500 °C for 10 min, showing negligible etching along grinding scratches in (a); slight formation of Co-rich (bright) spinel phase (denoted by s) along step ledges in (b) but not in (c); and onset intragranular/intergranular etching in (d).

ing along the grinding scratches (Fig. 5a). The Co-rich spinel phase along the terrace ledges was recognized for the C8M2 polycrystals annealed at 800 °C for 10 min (Fig. 5b) but not 1100 °C for 10 min (Fig. 5c). Slight thermal etching at grain boundaries and dislocation outcrops was recognized for the C8M2 ceramic sample annealed at a higher temperature of 1500 °C for 10 min. It can be concluded that the relatively refractory MgO component considerably suppressed thermal etching and formation of the Co-rich spinel phase in the temperature range studied.

3.3. Morphology of thermal etch pits and hillocks in C8M2 ceramics

SEM (SEI) at a relatively high magnification showed that the sintered C8M2 ceramic sample subject to annealing at 1500 °C for 10 min have trigonal thermal etch pits, which were significantly dragged by the inclined {1 1 1} ledge and {1 1 1}/{1 1 0} kinks when viewed in the ⟨1 1 1⟩ direction (Fig. 6a). The hexagonal etch pits with the inclined {1 1 1} and {1 0 0} walls in ⟨1 1 1⟩ zone axis were developed when the sample was subjected to further annealing at 1500 °C for 1 and 3 h (Fig. 6b and c, respectively). It should be noted that these etch pits preferentially occurred and coalesced at the {1 1 1} surface due to the outcrop of dislocations with a specific {1 1 0} line vector as discussed later.

In general, dislocation etch pit surrounded by shallow terraces was typical observed for the sample subject to short annealing at 1500 °C for 10 min (Fig. 7a). Circular terrace at the interior of the pit then developed upon annealing at 1500 °C for 1 h, presumably due to an onset diffusion-controlled etch process (Fig. 7b). The etch pits finally coalesced/impinged when the sample was annealed for a longer time up to 3 and 12 h as shown in Fig. 7c and d, respectively. The spiral hillocks and faceted pits were commonly observed for these specimens (Fig. 8).

3.4. Condensation of Co-rich crystallites on C8M2 ceramics

The sintered C8M2 ceramic sample subject to annealing at 1500 °C for 10 min showed the cube-like $Co_{1-x}O$ condensates, which gave bright contrast in SEM image and high Co counts in the point-count EDX spectrum (Fig. 9). It is difficult, if not

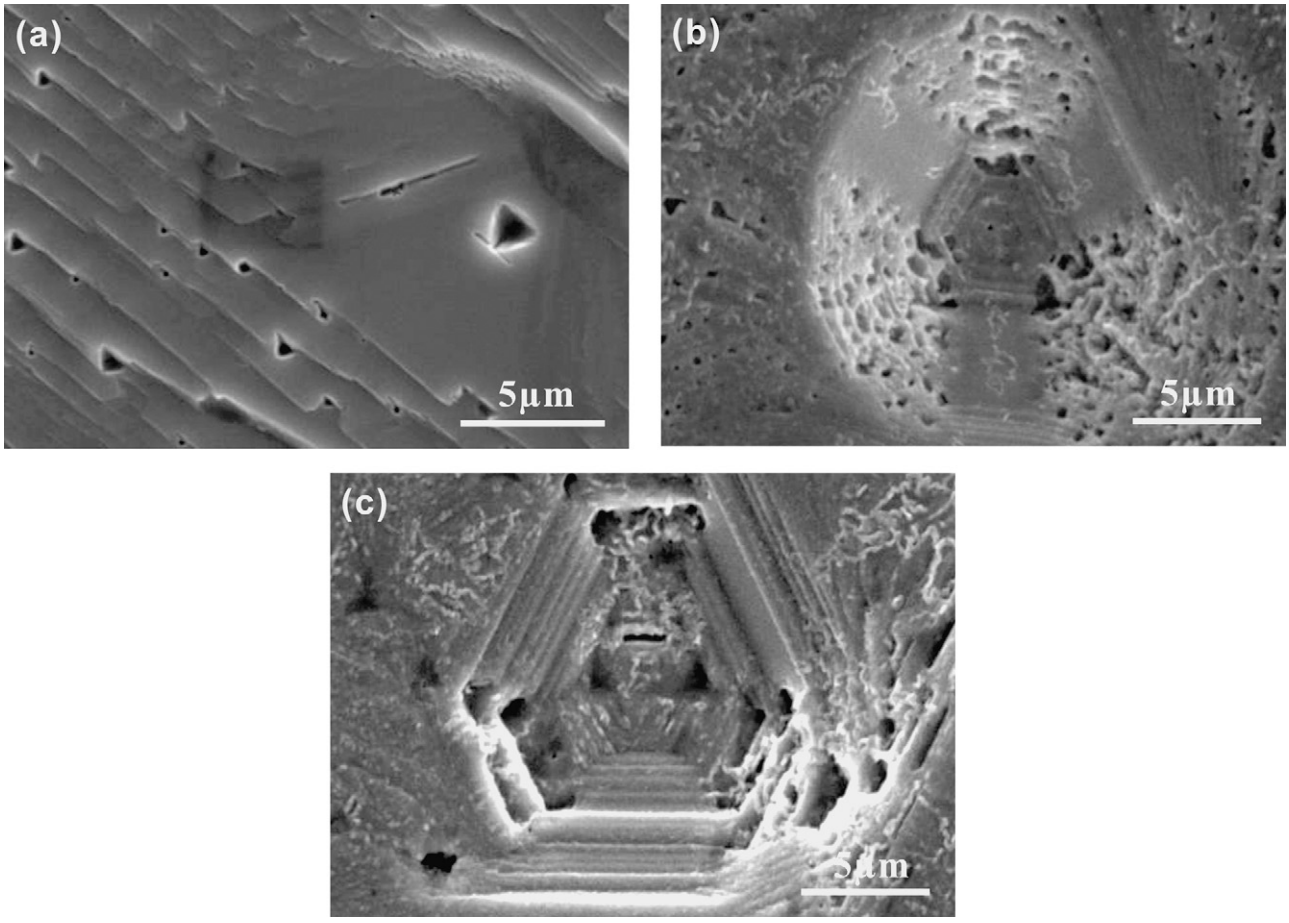

Fig. 6. Magnified SEM (SEI) of the sintered C8M2 sample subject to thermal etching at 1500 °C for (a) 10 min, (b) 1 h and (c) 3 h, showing etch pit dragging on inclined {1 1 1} ledge and {1 1 1}/{1 1 0} kinks in (a), and the coalescence of dislocation etch pits preferentially at inclined {1 1 1} surface due to {1 1 0} line vector of dislocations (cf. text) in (b) and (c).

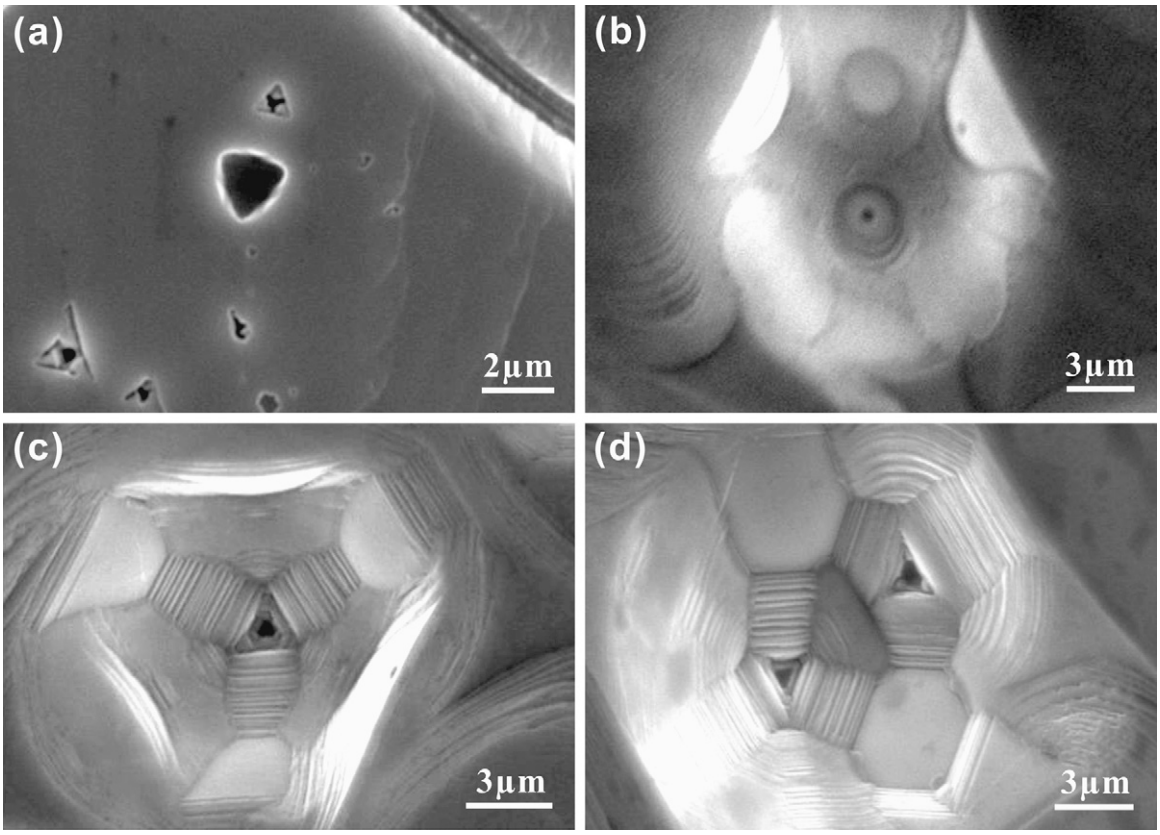

Fig. 7. SEM (SEI) of the sintered C8M2 sample subject to thermal etching at 1500 °C for (a) 10 min, (b) 1 h, (c) 3 h and (d) 12 h showing etch pit nucleation on dislocation outcrop to form deep pore within shallow etch pits. Note circular terrace within the pit due to onset diffusion-controlled etch process in (b), and coalescence of etch pits from (c) to (d) (cf. text).

possible, to do electron back-scattered diffraction on a thermally etched surface especially when covered with many micron-size $Co_{1-x}O$ condensates and terrace ledges. However, the orthogonal and equilateral {1 0 0} ledges of the underlying solid solution grain with cubic rock salt type structure (Fig. 9) indicate that it is in [0 0 1] zone axis. This approach of crystal orientation determination, based on thermal etch pits that reflect the internal crystal structure and surface energetics, was commonly accepted by researchers. Our additional experiment further indicates that the $Co_{1-x}O$ condensates typically have well-developed {1 0 0} surfaces (Appendix B). The crystallographic orientation of the $Co_{1-x}O$ condensates with respect to the underlying grain can, thus be unambiguously determined. In fact, the cubic $Co_{1-x}O$ condensates tended to have their edges parallel to, or 45° off, the orthogonal ledges of the terraces, indicating two specific epitaxial relationships as discussed later. This interpretation is in accordance with the interfacial energetics considerations and the well-known such relationships for the analogous fcc Au condensates on KCl(1 0 0) with or without steps as addressed in Section 4.4.

The C8M2 ceramic sample subject to thermal etching at 800 °C for 10 min also showed Co-rich phase at the step ledges (Fig. 10). This Co-rich phase is apparently the spinel formed by an oxidation precipitation process and/or the $Co_{1-x}O$ protoxide formed by a sublimation–condensation process. The nearby grain boundaries became precipitate-free valleys in such a sublimation–condensation process.

4. Discussion

4.1. Defect chemistry and spinel paracrystal formation in bulk material

A smaller X-ray lattice parameter for Mg-doped $Co_{1-x}O$ (0.4255 nm) than undoped $Co_{1-x}O$ (0.4260 nm) indicated that Mg^{2+} (effective ionic radii, 0.0720 nm) replaced Co^{2+} in high spin (0.0745 nm) rather than low spin state (0.0650 nm) in CN 6.[11] The undersized dopant Mg^{2+} in the Co^{2+} site could also force further cobalt ion to enter the interstitial site as $Co_i^{\bullet\bullet\bullet}$, which then induced charge-compensating cation vacancies and 4:1 defect clusters through the following equation in Kröger–Vink notation[12]:

$$MgO \xrightarrow{CoO} Mg_{Co}^{x} + [Co_i^{\bullet\bullet\bullet} + 4\,V_{Co}'' + 5h^{\bullet}] + O_o^{x} \quad (1)$$

Here Mg_{Co}^{x} signifies a noncharged magnesium at cobalt sites in the crystal lattice and h could be associated with V_{Co}'' to form V_{Co}' or associated with Mg_{Co}^{x} to form $Mg_{Co}^{\bullet}$. The resultant 4:1 type defect clusters can then be assembled to form paracrystalline ordered state and then spinel. According to previous TEM observations,[10] the Mg-dopant introduced extra cobalt vacancies and Co^{3+} interstitials for $Co_{3-\delta}O_4$ to form a smaller interspacing of paracrystal, i.e. 4.5 instead of 5.0 times that of average spinel lattice parameter. The δ value of Mg-doped

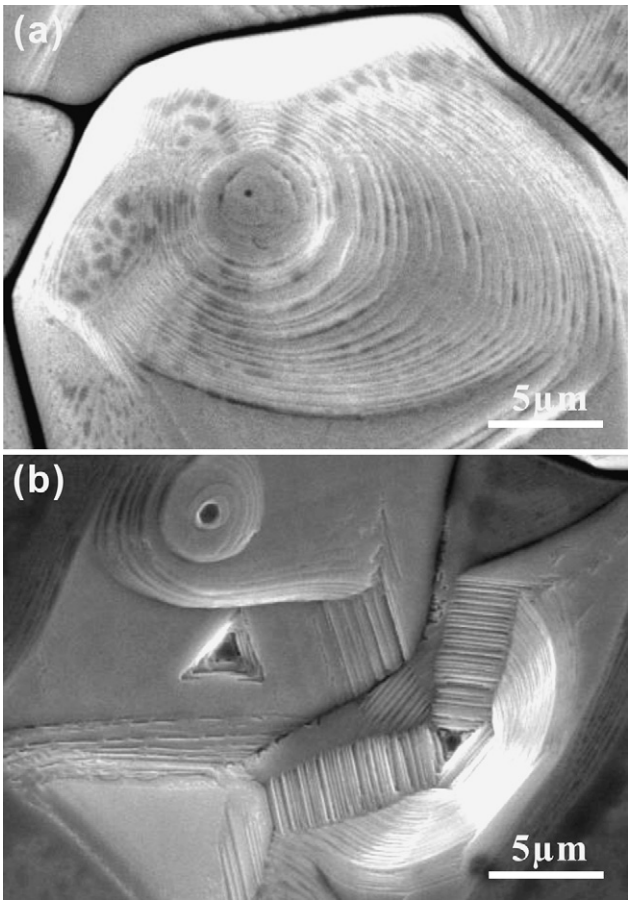

Fig. 8. SEM (SEI) of the sintered C8M2 sample subject to thermal etching at 1500 °C for (a) 3 h and (b) 12 h showing spiral hillock and nonspiral facetted pits.

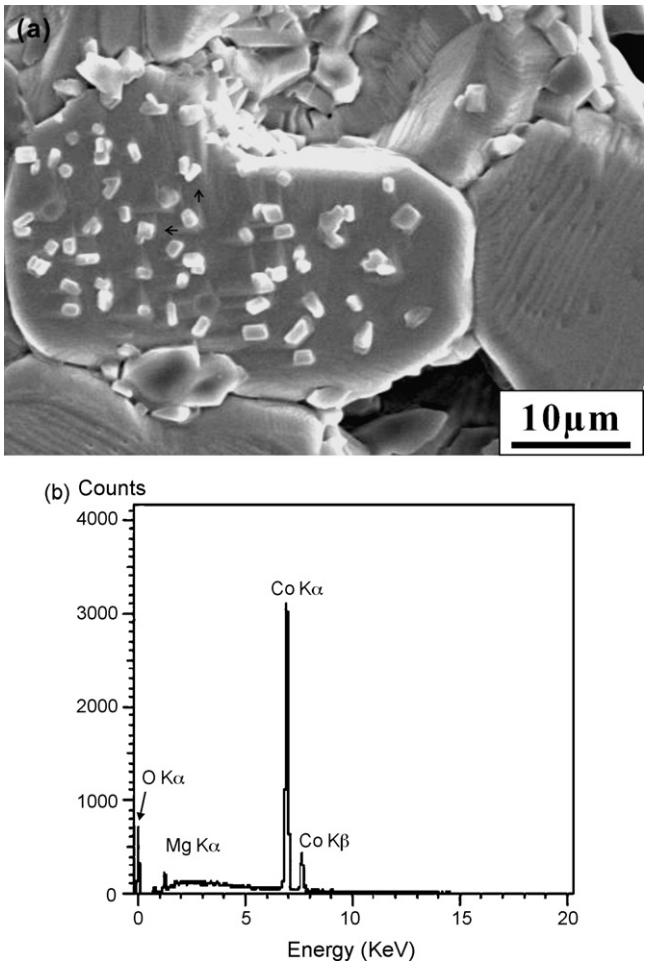

Fig. 9. SEM (a) SEI of the sintered C8M2 sample subject to thermal etching at 1500 °C for 10 min showing cube-like $Co_{1-x}O$ condensates (bright) with slight Mg counts from the substrate as indicated by point-count EDX spectrum in (b). The cubic $Co_{1-x}O$ condensates tended to have their edges parallel to, or 45° off, the orthogonal ledges (denoted by arrows) of the (1 0 0) terraces on the underlying solid solution grain, following two specific epitaxial relationships (cf. text).

$Co_{3-\delta}O_4$ was calculated to be ca. 1.37 times higher than undoped $Co_{3-\delta}O_4$.[13]

As mentioned, spontaneous oxidation of $Co_{1-x}O$ to form $Co_{3-\delta}O_4$ spinel occur below ca. 900 °C in air.[9] The intrinsic defects were generally believed to generate in the near-surface and dislocation regions for $Co_{1-x}O$ to nucleate $Co_{3-\delta}O_4$ spinel with paracrystalline distribution of defect clusters.[13] According to the phase diagram,[14] the $Co_{1-x}O$–MgO system forms complete solid solution at high temperatures in air and decomposes below ca. 850 °C into Mg-doped (<1 at.%) $Co_{3-\delta}O_4$ spinel and protoxide of a wide Co/(Mg + Co) atomic ratio. (From 850 to 600 °C in air, the protoxide that equilibrates with Mg-doped $Co_{3-\delta}O_4$ spinel has the atomic ratio Co/(Mg + Co) decreasing from 99% to ca. 2%.[14])

4.2. Solute segregation and spinel paracrystal formation at line and planar defects

According to ref.[10] and the present TEM observations (Fig. 3), the dislocation of the $Co_{1-x}O$–MgO solid solution has a line vector parallel to ⟨1 1 0⟩ directions. The Mg^{2+} solute segregation at dislocations may affect space charge and act as inhibitor for the nucleation of etch pit via sublimation and short-circuit diffusion of atoms.

Mg^{2+} segregation might be more pronounced at grain boundaries and free surface to affect the surface morphology upon high temperature annealing. In this connection, it is of interest to note that metal vacancy concentration can be higher near the grain boundary or free surface than in the bulk. For example, the nickel vacancy increases by a factor of about 40 over the bulk value for the (2 1 1)/[0 1 1] twist grain boundary of $Ni_{1-x}O$ at 727 °C.[15] The near-surface layers of Fe_2O_3,[16] and CoO[17] also have much larger deviations from stoichiometry and higher defect concentrations than the bulk. Due to this surface effect, the undoped $Co_{1-x}O$ sample suffered significant oxidation to form the spinel phase when annealed at both 800 and 1100 °C (Fig. 4b and c); whereas the $Co_{1-x}O$–MgO solid solution showed the spinel only when annealed at 800 °C but not 1100 °C (Fig. 5b and c). It is, thus conceivable that submicron-sized paracrystalline spinel phase in the sample annealed at 1500 °C (Fig. 2) was formed via an oxidation precipitation process near the surface and dislocation regions upon cooling below 1100 °C in air. Apparently, the surface morphology, as revealed by SEM at a

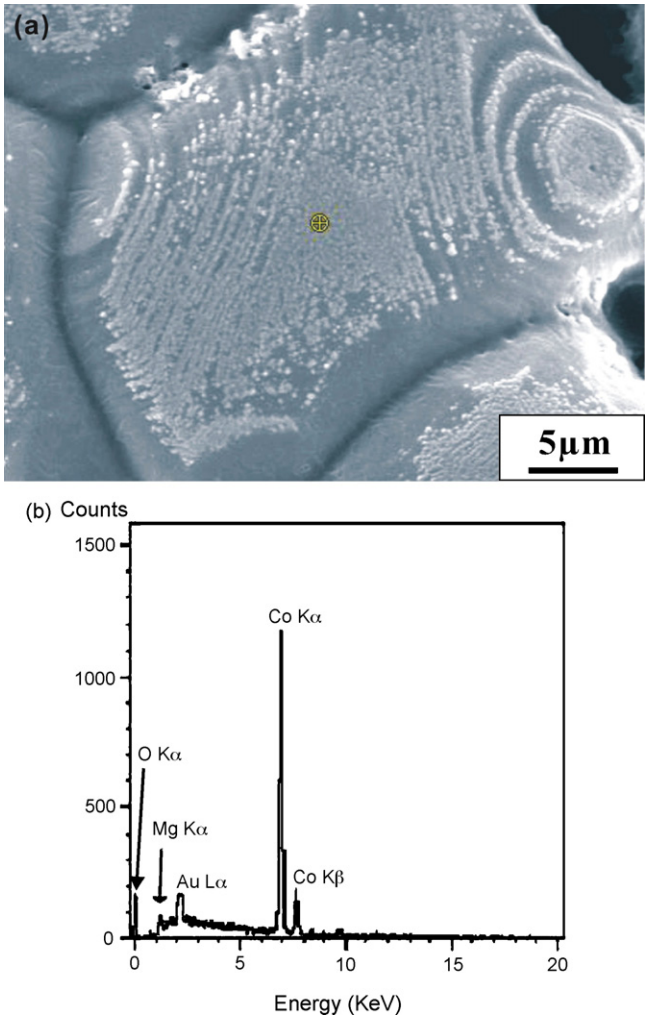

Fig. 10. Magnified SEM (a) SEI and (b) point-count EDX spectrum of the sintered C8M2 sample subject to thermal etching at 800 °C for 10 min. The precipitate-free valleys in (a) are due to grain boundary grooving and the Co-rich spinel precipitates (bright) at steps and ledges are due to an oxidation precipitation process (cf. text). The EDX spectrum taken from the area covered with the Co-rich spinel phase, as marked by a cross symbol in (a), shows Mg counts from the substrate.

much lower magnification, was affected more by dislocations than the paracrystalline state of the spinel.

4.3. Dislocation exposure and the formation of thermal etch pits with spiral hillocks

Impurity inhibitors were known to help nucleate etch pits on special oriented dislocation outcrops on a specific surface for a number of hexagonal ceramic crystals upon acidic dissolution or thermal etching as mentioned. Dissolution of willemite single crystal at low pH indicated that impurities inherent in nature or added deliberately to the etching solution, affect the incubation time of etch pit formation at dislocation outcrops.[2] This was rationalized by the varied poisoning effect on dislocation outcrops, in particular Fe^{2+} to maintain near-surface undersaturation of willemite, as essential to nucleate etch pits.[2] As for thermal etching of willemite at 1250 °C, i.e. homologous temperature $T/T_m = 0.85$ (where T_m is the congruent melting temperature 1512 °C of willemite), such impurities were suggested to segregate to dislocation outcrops both via lattice diffusion and viscous flow during surface premelting.[5] On the other hand, Mn significantly suppressed the formation of thermal etch pits at dislocations and subgrain boundaries of the polycrystalline willemite.[6] As for the present nucleation of thermal etch pits at the dislocations of the $Co_{1-x}O$–MgO solid solution, it was presumably the accumulation of refractory component Mg^{2+} and other tramp impurities at dislocation outcrops to ensure near-surface undersaturation of the protoxide to nucleate etch pit.

The outcrops of ⟨1 1 0⟩ aligned dislocations are also of concern to the nucleation of etch pit openings with triangular and/or hexagonal shape on {1 1 1} of the $Co_{1-x}O$–MgO solid solution. The triangular etch pit on {1 1 1} surface, as observed in the incipient stage, typically has a flat base except a drastic deepening along the dislocation core (Figs. 6a and 7a). This indicated that the thermal etching rates along the principal directions have the following relationship ⟨1 1 0⟩ > ⟨1 1 1⟩ > ⟨1 1 2⟩, in accord with the order of decreasing *d*-spacing or increasing bonding strength of the protoxide. The hexagonal etch pits developed in later stage consist of the inclined {1 1 1} and {1 1 1} surfaces (Fig. 6b and c), which intersect at an angle of 35.26° and 0°, respectively with the ⟨1 1 0⟩ directions as shown in the (1 1 1) stereographic projection (Fig. 11a). Since ⟨1 1 0⟩ are closer to the plane normal of {1 1 1} than {1 0 0}, the ⟨1 1 0⟩ aligned dislocations would outcrop on the {1 1 1} rather than {1 0 0} surfaces. This was indeed observed in Figs. 6b and c and depicted schematically in top view and cross section in Fig. 11b and c, respectively. Note the inclined {1 0 0} surface of the etch pits may consist of alternating facets family of {1 1 1}, whereas the inclined {1 0 0} surface have alternating {1 1 1}/{1 0 0} facets, in accord with the cubo-octahedral habit of the negative crystal. Due to thermal migration of such dislocations and the dragging effect of predominant {1 1 1} facets (Fig. 6a), the etch pit openings tended to assemble and coalesce as shown in Fig. 6b and c.

As for randomly-oriented grain boundaries, their near edge-on exposure is expected to facilitate Co sublimation for the $Co_{1-x}O$–MgO solid solution and undoped $Co_{1-x}O$ sample to form deep grooving as shown in Figs. 3d and 2d, respectively. The surface morphology was complicated by the migration of dislocations and grain boundaries at a moderate high homologous temperature (such as $T/T_m = 0.74$ at 1500 °C for $Co_{1-x}O$–MgO solid solution) under the space charge effect. (Space charge may exert considerable Coulombic interactions on dislocations and grain boundaries to affect their mobility as experimentally proved for a number of oxide ceramics.[18])

The impurity segregation at dislocation also accounts for the formation of thermal etch hillocks at the center of hexagonal etch pits analogous to the formation of thermal etch hillock of willemite.[5] (The hillocks near the center of hexagonal pits of willemite were suggested to be a result of segregation of inhibitors at dislocation cores during thermal etching.[5]) The spiral hillocks of $Co_{1-x}O$–MgO solid solution (Fig. 8) can be attributed to spiral growth via dislocations more or less with screw nature along the ⟨1 1 0⟩ line vector.

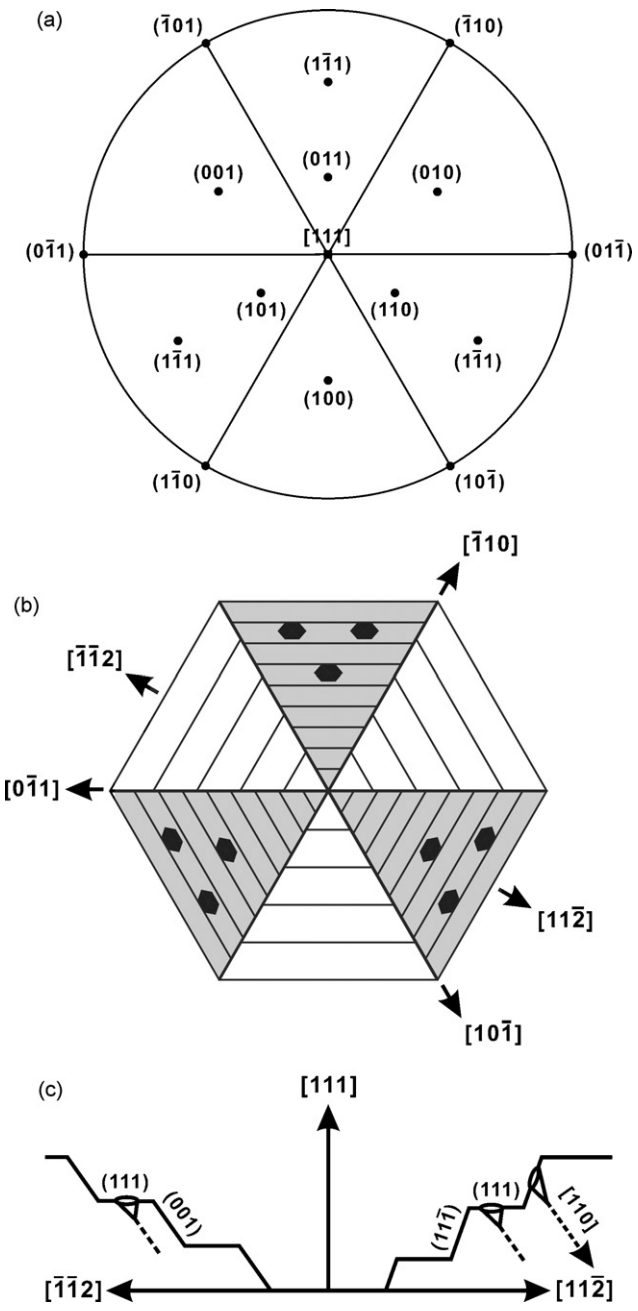

Fig. 11. (a) (1 1 1) stereographic projection of $Co_{1-x}O$–MgO solid solution with rock salt type structure showing the plane normals {1 1 0} are closer to {1 1 1} than {1 0 0}, (b) corresponding etch pit drawing showing the inclined {1 1 1} surfaces (gray), but not the inclined {1 0 0} surfaces (white), have smaller-size etch pits nucleated at the outcrops of ⟨1 1 0⟩-aligned dislocations and (c) cross section of (b) along ⟨1 1 2⟩ showing the ⟨1 1 0⟩-aligned dislocations tend to outcrop at the inclined {1 1 1} surface (right) with stepwise {1 1 1} facets, but not ourcrop at the inclined {1 0 0} surface (left) with stepwise {1 1 1}/{1 0 0} facets (cf. text).

The etch pit opening with well-developed {1 1 1} and/or {1 0 0} walls suggested that an interface-reaction-controlled process was valid at open area of $Co_{1-x}O$–MgO solid solution. However, at the tips of some etch pits (Fig. 7b) and hillocks (Fig. 8a), a diffusion-controlled process might prevail instead.

4.4. Epitaxial condensation of $Co_{1-x}O$ on $Co_{1-x}O$–MgO solid solution grain

The $Co_{1-x}O$ condensates (denoted as c) with cube-like shape were parallel aligned or 45° off with respect to the orthogonal {1 0 0} ledges of the underlying $Co_{1-x}O$–MgO solid solution grain (denoted as cm) indicating that the crystallites have parallel or 45° off epitaxial relationship with the substrate. Fig. 12a and

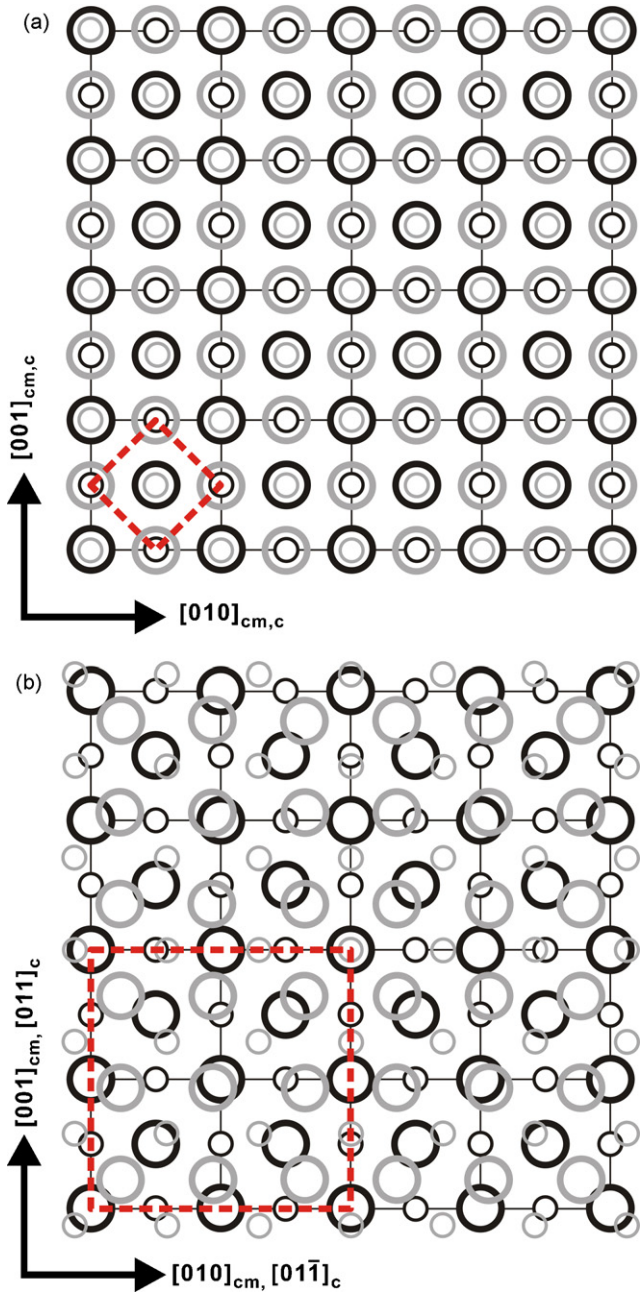

Fig. 12. Schematic drawing (top view) of the $(1\,0\,0)_c/(1\,0\,0)_{cm}$ interface for the $Co_{1-x}O$ (gray open circle, denoted as c) condensate having (a) parallel and (b) 45° crystallographic relationships with the underlying crystal of $Co_{1-x}O$–MgO solid solution (black open circle, denoted as cm). Cation and anion positions as denoted by small and big circles, respectively, are based on the lattice parameters (cf. text). The coincidence site lattice as defined by the superimposition of cations and anions for a beneficial Coulombic interaction is denoted by red dotted line.

b show that there is a smaller coincidence site lattice (CSL), i.e. a better match of cations and anions for a beneficial Coulombic interaction, at the $(1\,0\,0)_c/(100)_{cm}$ interface for the parallel than the 45° off relationship. In other words, the parallel epitaxial relationship is the energy cusp, whereas the 45° relationship is a local and secondary energy minimum.

Apparently the epitaxial $Co_{1-x}O$ crystallites were formed via a sublimation–condensation process for the less inert component, i.e. $Co_{1-x}O$ of the protoxide solid solution. It is hard, if not impossible, to envisage two epitaxial relationships if the crystallites were deposited atom-by-atom on the substrate. On the other hand, the epitaxial bifurcation can be reasonably explained by cube-like condensates being formed in the first place and then assembled via a Brownian motion/coalescence process upon deposition on the $\{1\,0\,0\}$ substrate until the two epitaxial relationships were reached independently. In this regard, it is of interest to note that thermally activated Brownian motion of fcc crystallites was known to occur over single crystal substrate, KCl(1 0 0) with or without steps until specific epitaxial relationships were reached.[19–24] The experimental results of Masson et al.[19] were further interpreted[24] with regard to the rotation behavior of non-epitaxial Au crystallites on a KCl (1 0 0) substrate, which developed into primary epitaxy ($[1\,1\,1]_{Au}//[1\,0\,0]_{KCl}$; $[1\,\bar{1}\,0]_{Au}//[0\,1\,0]_{KCl}$, and "second" epitaxy (in fact $[1\,0\,0]_{Au}//[1\,0\,0]_{KCl}$; $[0\,1\,0]_{Au}//[0\,1\,0]_{KCl}$ and $[1\,0\,0]_{Au}//[1\,0\,0]_{KCl}$; $[0\,1\,0]_{Au}//[0\,1\,1]_{KCl}$). The size and temperature dependence of diffusivity of the crystallites has been measured over KCl(1 0 0) and found to be in accordance with Brownian-type motion of the crystallites in terms of interfacial diffusion of atoms from leading edge to trailing edge of the crystallites.[19] Einstein's molecular theory of heat,[25] Eyring's transition-state model[26] and frictional force at a viscous interface were, thus adopted to formulate the diffusivity equation of the crystallite over the single crystal substrate.[20–22] Following this Brownian motion scenario, we suggest that the cation–anion mixed $\{1\,0\,0\}$ surfaces of the $Co_{1-x}O$–MgO solid solution grain may facilitate Co sublimation and subsequent deposition-assembly of the cubic $Co_{1-x}O$ condensates to form energetically favorable $(1\,0\,0)_c/(1\,0\,0)_{cm}$ interface under little influence of the relatively inert Mg^{2+} solute.

5. Conclusions

1. The solid solution of MgO in polycrystalline $Co_{1-x}O$ considerably suppressed the thermal etching and the formation of Co-rich spinel in the temperature range of 400–1500 °C in air.
2. Prolonged annealing of $Co_{1-x}O$–MgO solid solution at 1500 °C caused anisotropic development of $\{1\,1\,1\}/\{1\,0\,0\}$-faceted etch pits/hillocks due to predominant exposure of $\langle 1\,1\,0\rangle$ oriented dislocations on the $\{1\,1\,1\}$ surfaces.
3. Cube-like $Co_{1-x}O$ crystallites were deposited preferentially on the (1 0 0) surface following parallel or 45° off crystallographic relationship with the underlying MgO–$Co_{1-x}O$ solid solution when thermally etched at 1500 °C.
4. The epitaxial bifurcation can be rationalized by Brownian motion of the cube-like $Co_{1-x}O$ condensates on the well-developed $\{1\,0\,0\}$ surfaces of the underlying crystal of $Co_{1-x}O$–MgO solid solution.

Acknowledgments

We thank an anonymous referee for helpful comments. This research is supported by Center for Nanoscience and Nanotechnology at NSYSU and Nanotechnology at NSYSU.

Appendix A

CoO–MgO phase diagram after Robin (1955).[14]

Appendix B

Lattice image of a typical $Co_{1-x}O$ condensate with well-developed $\{1\,0\,0\}$ surfaces. The condensate was fabricated by pulsed Nd-YAG laser ablation on Co target at 1.5×10^8 W/cm^2 power density under 50 L/min oxygen flow rate in air.

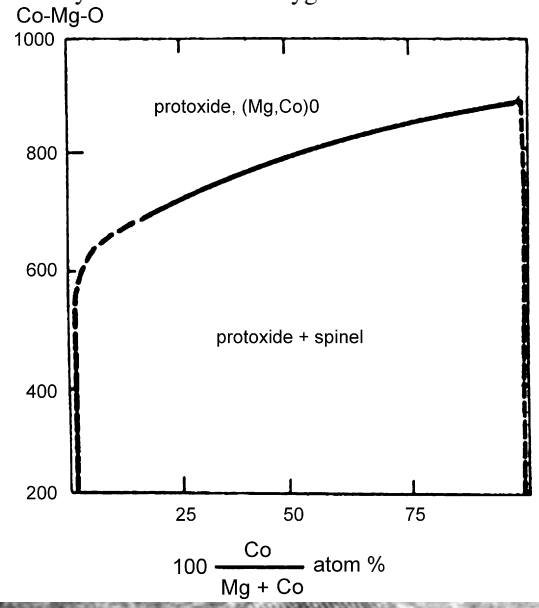

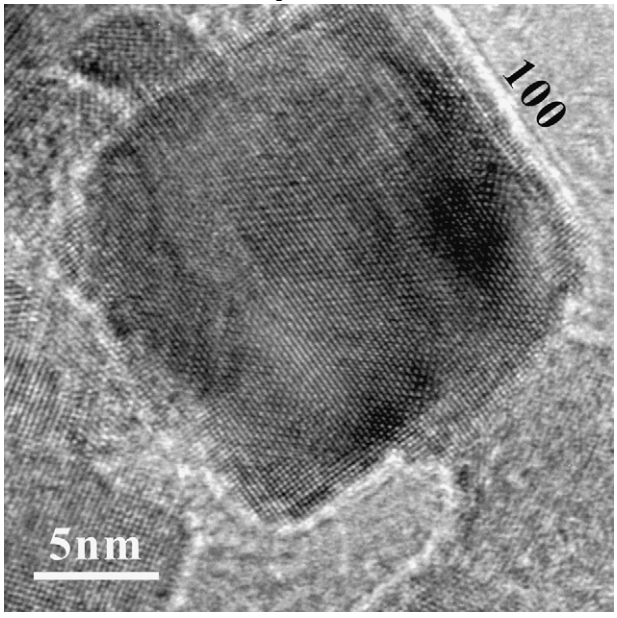

References

1. Lin, C. C. and Shen, P., Directional dissolution kinetics of willemite. *Geochim. Cosmochim. Acta*, 1993, **57**, 27–35.
2. Lin, C. C. and Shen, P., Incubation time of etch pits at dislocation outcrops. *Geochim. Cosmochim. Acta*, 1995, **59**, 2955–2963.
3. Lin, C. C. and Shen, P., Role of screw axes in dissolution of willemite. *Geochim. Cosmochim. Acta*, 1993, **57**, 1649–1655.
4. Tseng, W. J., Lin, C. C., Shen, P. W. and Shen, P., Directional/acidic dissolution kinetics of (OH, F, Cl)-bearing apatite. *J. Biomed. Mater. Res.: Part A.*, 2006, **76**, 753–764.
5. Chao, P. T., Shen, P. and Lin, C. C., Thermal cycle etching of willemite (0 0 0 1): effects of surface premelting, dislocation outcrops and polygonization. *Mater. Sci. Eng. A*, 2002, **335**, 191–197.
6. Chang, C. C. and Shen, P., Thermal-etching development of α-Zn_2SiO_4 polycrystals. *Mater. Sci. Eng. A*, 2000, **288**, 42–46.
7. Woodcock, S. and Leyland, J. D., The choice of phosphor for modern CRT display applications. *Display*, 1979(July), 69–82.
8. Zwinkels, M. F. M., Jaras, S. G., Menon, P. G. and Griffin, T. A., Catalytic materials for high temperature combustion. *Catal. Rev. Sci. Eng.*, 1993, **35**, 319–358.
9. Oku, M. and Sato, Y., In situ X-ray photoelectron spectroscopic study of the reversible phase transition between CoO and Co_3O_4 in oxygen of 10^{-3} Pa. *Appl. Surf. Sci.*, 1992, **55**, 37–41.
10. Tsai, T. M., Yang, K. C. and Shen, P., Defect clusters and precipitation/oxidation of MgO–$Co_{1-x}O$ solid solution. *J. Solid State Chem.*, 2004, **177**, 3301–3309.
11. Shannon, R. D., Revised effective ionic radii and systematic studies of interatomic distances in halides and chalcogenides. *Acta Cryst. A*, 1976, **32**, 751–767.
12. Kröger, F. A. and Vink, H. J., Relations between the concentrations of imperfections in crystalline solids. *Solid State Phys.*, 1956, **3**, 307–435.
13. Lee, W. H. and Shen, P., $Co_{3-\delta}O_4$ paracrystal: 3-D assembly of nano-size defect clusters in spinel lattice. *J. Solid State Chem.*, 2004, **177**, 101–108.
14. Robin, J., Constitution and stability of several solid solutions based on cobalt oxide. *Ann. Chim. (Paris)*, 1955, **10**, 389–412.
15. Duffy, D. M., A calculation of the formation energies of intrinsic defects near grain boundaries in NiO. *Phil. Mag.*, 1984, **50**, 143–154.
16. Gleitzer, C., Nowotny, F. and Rekas, M., Surface and bulk electrical properties of the hematite phase Fe_2O_3. *Appl. Phys. A*, 1991, **53**, 310–316.
17. Nowotny, J., Sikora, I. and Wagner Jr., J. B., Segregation and near-surface diffusion for undoped and Cr-doped CoO. *J. Am. Ceram. Soc.*, 1982, **65**, 192–196.
18. Hwang, S. L. and Chen, I. W., Grain size control of tetragonal zirconia polycrystals using the surface charge concept. *J. Am. Ceram. Soc.*, 1990, **73**, 3269–3277.
19. Masson, A., Métois, J. J. and et Kern, R., Migration brownienne de cristallites sur une surface et relation avec l'épitaxie I. partie expérimentale. *Surf. Sci.*, 1971, **27**, 463–482.
20. Kern, R., Masson, A. and et Métois, J. J., Migration brownienne de cristallites sur une surface et relation avec l'épitaxie II. partie théorique. *Surf. Sci.*, 1971, **27**, 483–498.
21. Métois, J. J., Gauch, M., Masson, A. and et Kern, R., Migration brownienne de cristallites sur une surface et relation avec l'épitaxie III cas de l'aluminium sur KCl: précisions sur le méchanisme de glissement. *Surf. Sci.*, 1972, **30**, 43–52.
22. Métois, J. J., Gauch, M., Masson, A. and et Kern, R., Épitaxie: phenomène de postnucleation sur L'exemple des couches minces discontinues d'aluminium et d'or sur (1 0 0) KCl. *Thin Solid Films*, 1972, **11**, 205–218.
23. Métois, J. J., Migration brownienne de cristallites sur une surface et relation avec l'épitaxie IV. mobilité de cristallites sur une surface: décoration de gradins monoatomiques de surface. *Surf. Sci.*, 1973, **36**, 269–280.
24. Kuo, L. Y. and Shen, P., On the rotation of nonepitaxy crystallites on single crystal substrate. *Surf. Sci.*, 1997, **373**, L350–L356.
25. Einstein, A., In *Investigations on the Theory of the Brownian Movement*, ed. R. Fürth. Methuen, 1926. pp. 1–24 [Translated from German into English by Cowper, A.D.].
26. Gladstone, S., Laidler, K. and Eyring, H., *The Theory of Rate Processes*. McGraw-Hill, New York, 1941.